**DTU Library**

# Transition from stochastic events to deterministic ensemble average in electron transfer reactions revealed by single-molecule conductance measurement

Li, Yueqi; Wang, Hui; Wang, Zixiao; Qiao, Yanjun; Ulstrup, Jens; Chen, Hong-Yuan; Zhou, Gang; Tao, Nongjian

# Transition from stochastic events to deterministic ensemble average in electron transfer reactions revealed by single-molecule conductance measurement

Yueqi Li[a], Hui Wang[b], Zixiao Wang[b], Yanjun Qiao[c], Jens Ulstrup[d], Hong-Yuan Chen[b,1], Gang Zhou[c,1], and Nongjian Tao[a,b,1]

[a]Center for Bioelectronics and Biosensors, Biodesign Institute, Arizona State University, Tempe, AZ 85287-5801; [b]State Key Laboratory of Analytical Chemistry for Life Science, School of Chemistry and Chemical Engineering, Nanjing University, 210023 Nanjing, China; [c]Laboratory of Advanced Materials, State Key Laboratory of Molecular Engineering of Polymers, Fudan University, 200438 Shanghai, China; and [d]Department of Chemistry, Technical University of Denmark, DK-2800 Kgs. Lyngby, Denmark

Electron transfer reactions can now be followed at the single-molecule level, but the connection between the microscopic and macroscopic data remains to be understood. By monitoring the conductance of a single molecule, we show that the individual electron transfer reaction events are stochastic and manifested as large conductance fluctuations. The fluctuation probability follows first-order kinetics with potential dependent rate constants described by the Butler–Volmer relation. Ensemble averaging of many individual reaction events leads to a deterministic dependence of the conductance on the external electrochemical potential that follows the Nernst equation. This study discloses a systematic transition from stochastic kinetics of individual reaction events to deterministic thermodynamics of ensemble averages and provides insights into electron transfer processes of small systems, consisting of a single molecule or a small number of molecules.

electron transfer reactions | single molecule | molecular electronics | stochastic electron transfer | ensemble averaging

Electron transfer is crucial in a wealth of chemical and biological processes and also in a wide range of applications, including materials synthesis, energy conversion, catalysis, and electrochemical sensors (1–3). Electron transfer reactions are by far most commonly studied by measuring the collective behavior of a large number of molecules. Single-molecule studies based on fluorescent spectroscopy (4–7) and force spectroscopy (8–10) have been developed. In contrast, electrical measurements (11–14), which are particularly suitable for electron transfer reactions as they probe an electron transfer process directly, are much less studied. Electrical measurements of single molecules require well-defined and strong electronic coupling between a redox molecule and two probing electrodes. This was achieved, for example, by the scanning tunneling microscopy (STM) break junction technique (15, 16), which bridges a molecule covalently between a STM tip and a substrate via molecular linkers. The molecular linkers provide robust electronic coupling between redox molecule and the electrodes, and changing the type and length of the molecular linkers allows systematic control of the electron transfer rate in and out of the redox center (17, 18). Using this technique, electron transfer reactions have been investigated by analyzing the average conductance of single molecules (16, 19–26), but there is a need to study single-electron transfer reaction events and transition from the behavior of individual molecules to that of a bulk collection of molecules. Such studies will help in bridging stochastic single-electron transfer reactions with deterministic thermodynamics based on the ensemble average of a large number of single-molecule reaction events and molecules.

Here we report a study of individual electron transfer reaction events in a single redox molecule by recording the conductance of the molecule vs. the potential with an electrochemical STM break junction method and analyze the connection between the stochastic single-reaction events and the ensemble average of a large number of reaction events (20). We show that the conductances of the molecule in the oxidized and reduced states are distinctly different and that measuring the conductance changes allows tracking of the individual single-molecule oxidation and reduction events. We vary the molecular linker length to change systematically the rate of electron transfer between the electrodes and the redox molecule and study the dependence of the electron transfer reaction on increasing molecular bridge length. We have further framed the experimental observations by numerical simulations based on first-order kinetics with the interfacial electrochemical rate constant described by the Butler–Volmer relation.

## Results and Discussion

We studied the electron transfer reactions of a series of ferrocene compounds, each consisting of a ferrocene redox center with two symmetrical alkane thiol linkers of different lengths (Fig. 1A). The thiol terminals can bind strongly to a gold STM tip and a gold STM substrate (27) to form a molecular junction, allowing the study of electron transfer in and out of the redox center (28). The length of the alkanethiols was varied by changing the number of $CH_2$ groups

### Significance

**Electron transfer (ET) is an elementary step in many chemical reactions and biological processes. Measuring ET at the single-molecule level opens new prospects for studying individual reaction steps and heterogeneity in ET. Despite recent advances, the connection between the single-molecule behavior and the ensemble averages remains unclear. By performing direct electrical measurements on ferrocene with variable lengths of molecular linkers, we found that the ET process is stochastic and follows first-order kinetics at the single-molecule level, but ensemble averaging of the single-molecule measurements recovers the thermodynamic behavior. This study provides a framework to connect stochastic single-molecule behavior and deterministic ensemble thermodynamics.**
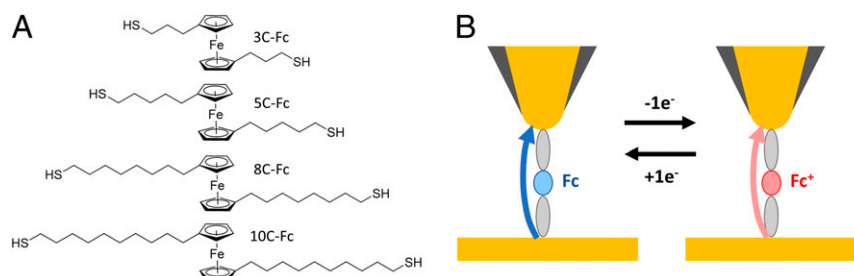
**Fig. 1.** (A) Structures of ferrocene compounds. (B) Scheme of charge transport through a ferrocene molecule that switches between oxidized and reduced states. The probability of the redox switching (electron transfer reactions) is controlled by the STM electrode potentials (tip and substrate) with respect to a reference electrode (silver wire) in an electrolyte.

in the alkanes. We denote the ferrocene compounds as nC-Fc, where $n = 3, 5, 8,$ and $10$ represents the number of $CH_2$ groups in the alkane bridges (see *SI Appendix,* Figs. S1–S4 for $^1H$ NMR spectra and *SI Appendix,* section 1 for synthesis procedures). We monitored the electron transfer reactions in single nC-Fc molecules by recording the conductance and controlled the reactions by varying the electrode potential (Fig. 1*B*; see *Materials and Methods* for details). The setup allowed us to control the potentials of both the STM tip and the substrate electrodes independently with respect to a reference electrode, as well as the bias voltage between the two STM electrodes. We performed the measurements in two ways: one was to determine the ensemble average of single-molecule conductance from repeated single-molecule measurements and the second one was to follow the stochastic electron transfer reaction events in single molecules.

We first examined the electron transfer reactions of nC-Fc molecules assembled on a gold substrate (see *Materials and Methods* for details) by cyclic voltammetry in acetonitrile with 0.1 M tetrabutylammonium tetrafluoroborate (TBA $BF_4$) as electrolyte (*SI Appendix,* Fig. S5 *A–D*). Each cyclic voltammogram exhibits a pair of peaks associated with the oxidation and reduction of the molecules. The peak heights are proportional to the potential sweep rate, indicating that the redox molecules are immobilized on the electrode surface (*SI Appendix,* Fig. S5 *E* and *F*). We determined the surface coverage of each nC-Fc from the peak areas and the equilibrium potential from the peak positions

(*SI Appendix,* Fig. S5 *A–D*). We refer to all of the potentials in this work with respect to the equilibrium potentials.

We determined the average conductance of single nC-Fc molecules by repeatedly measuring the single-molecule conductance at a fixed potential (21) and studied the potential dependence by holding the potential at different values. The conductance histogram of 3C-Fc obtained from the individual measurements at −0.08 V is plotted in Fig. 2*A*, showing a peak around 0.02 $G_0$, where $G_0$, the conductance quantum, is $7.748 \times 10^{-5}$ S. Since this potential was well below the equilibrium potential, there is 95% probability that the molecule is in the reduced state according to the Nernst equation and the recorded cyclic voltammograms. We thus conclude that the average conductance of a 3C-Fc molecule in the reduced state is 0.02 $G_0$. When we increased the potential to 0.12 V, well above the equilibrium potential, the average conductance of the molecule shifted to the higher value of 0.13 $G_0$ as shown in the corresponding conductance histogram (Fig. 2*B*). At 0.12 V, there is 99% probability that the molecule is in the oxidized state and we attribute 0.13 $G_0$ as the average conductance of a 3C-Fc molecule in this state. The increase in the single-molecule conductance associated with oxidation accords with previous reports (16, 24) and is supported by UV-Vis spectroscopy, which reveals an increased absorption wavelength (smaller energy gap between the highest occupied molecular orbital and lowest excited state) (29) for the oxidized form than for the reduced form.
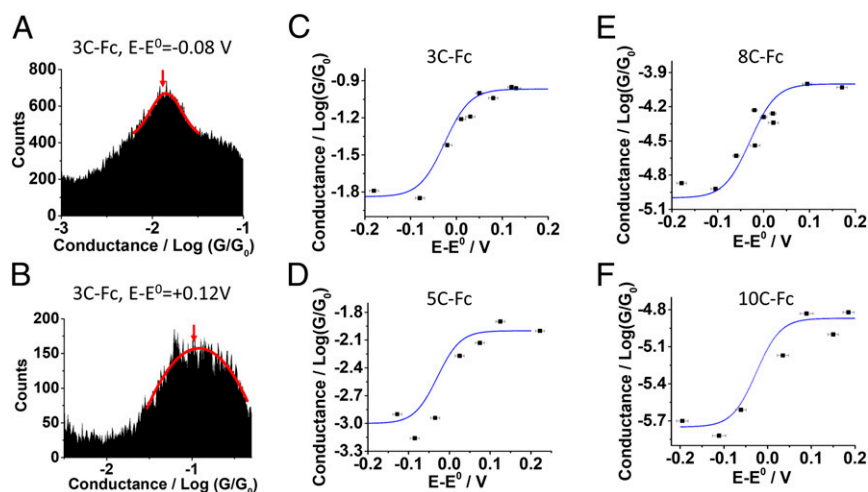


**Fig. 2.** Average conductance of a ferrocene molecule and its dependence on potential. (*A* and *B*) Conductance histograms of 3C-Fc measured at overpotentials of −0.08 V (*A*) and +0.12 V (*B*), respectively, showing an increase in the average conductance associated with switching of the molecule from the reduced to the oxidized state. The red curves are Gaussian fittings of the conductance peaks and the red arrows mark the peak positions. (*C–F*) Plots of averaged conductance vs. overpotential for (*C*) 3C-Fc, (*D*) 5C-Fc, (*E*) 8C-Fc, and (*F*) 10C-Fc. The blue curves are sigmoidal fittings of the data according to probabilities determined by the Nernst equation.

To study the electron transfer reaction of the molecule further, we varied the potential systematically from low to high values and plotted the average conductance against potential, which reveals a sigmoidal dependence of the conductance on the electrochemical potential (Fig. 2C). This sigmoidal dependence differs from that in most previous work, which reported a peak in the conductance vs. potential plot according with incoherent two-step sequential hopping (22, 25, 30–32), coherent one-step tunneling (33–37), or a fast coherent/incoherent channel coupled with a low hopping-rate redox channel (38–40). The former rests on the assumption that an electron (or a hole) hops from one electrode to the molecule first and then out of the molecule to the second electrode after losing its phase coherence (i.e., full vibrational relaxation of the molecule in the intermediate electronic state). In the latter model, an electron (or hole) tunnels through the molecule coherently via the reduced or oxidized state of the molecule without or with only partial loss of phase coherence. Both models predict a maximum in conductance vs. potential, which cannot explain sigmoidal dependence of the conductance on potential. Coupling of an electron transfer event to a low-frequency "soft" nuclear coordinate could, however, lead to sigmoidal dependence (15), but this is mechanism is unlikely here as we discuss later.

The above models imply that the electron transport is mediated by sequential or coherent electron transfer via redox states of the molecule. The conductance of the molecule is therefore closely related to the interfacial electrochemical electron transfer rates (oxidation and reduction) in the tunneling gap. When these contributions are small, the conductance is, however, instead determined by electron tunneling through the molecule, which is in either the oxidized or the reduced state, corresponding to superexchange via a low-lying intermediate state at the redox center (1) (see *SI Appendix*, section 2 for a detailed discussion). This process was considered by Kuznetsov (41), but has not been systematically examined experimentally. In this case the average conductance of the redox molecule, <G>, defined as <G> = I/bias voltage, where bias is a small fixed value (0.1 V), is given by (41)

$$<G> = G_{ox}C_{ox} + G_{red}C_{red},$$ [1]

where $G_{ox}$, $C_{ox}$ and $G_{red}$, $C_{red}$ are the conductance values and probabilities of the molecule in the oxidized and reduced states, respectively. $C_{ox}$ and $C_{red}$ are related by

$$C_{ox} + C_{red} = 1$$ [2]

and their potential dependence given by the Nernst Equation,

$$\frac{C_{ox}}{C_{red}} = \exp\left[-\frac{e}{k_BT}(E - E_0)\right],$$ [3]

where $e$ is the electron charge, $k_B$ is the Boltzmann constant, $T$ is the temperature, $E$ is the STM electrode potential, and $E_0$ is the equilibrium potential. Substituting Eqs. 2 and 3 into Eq. 1 leads to sigmoidal dependence of the conductance on the potential given by

$$<G> = G_{red} + \frac{1}{1 + \exp\left[\frac{e}{k_BT}(E - E_0)\right]}(G_{ox} - G_{red}).$$ [4]

Taking the conductance values ($G_{ox}$ and $G_{red}$) in the oxidized and reduced states from the conductance measurements at potentials well above or below the equilibrium potential, we calculated the potential dependence of the average conductance using Eq. 4 and found excellent agreement with the experimental data for 3C-Fc (Fig. 2C). We then repeated the same analysis for 5C-Fc, 8C-Fc, and 10C-Fc and found that Eq. 4 describes the measured potential dependence of the average conductance well in

all of the cases (Fig. 2 D–F). These model calculations do not have any fitting parameters, and the quantitative agreement between the measured conductance values and Eq. 4 supports that the conductance of nC-Fc with different molecular linker lengths is primarily due to electron tunneling through the molecule without direct redox mediation, and the molecule is in either the reduced or the oxidized state, depending on the potential. It also shows that the potential dependence of the single-molecule conductance averaged over repeatedly measured individual molecules follows the equilibrium thermodynamics described by the Nernst equation.

Next, we turned to the study of individual electron transfer events in single molecules. We performed the experiment by first pushing the STM tip into contact with the nC-Fc covered substrate and then retracting the tip from the substrate and monitoring the conductance during these steps. When the conductance fell to a plateau (*SI Appendix*, Fig. S6), indicating that a nC-Fc molecular bridge between the STM tip and the substrate had formed, we stopped the STM tip motion, swept the potential, and monitored the conductance during the potential sweep. In each potential sweep, the potential started from a sufficiently negative (positive) value and ended at a sufficiently positive (negative) value to ensure that the molecule started in the reduced (oxidized) state and ended in the oxidized (reduced) state.

We monitored the oxidation by tracking the conductance change in the molecule. Fig. 3 A–C shows several representative single-molecule conductance vs. overpotential curves for 3C-Fc. Overall, the conductance in all of the curves increases with increasingly positive potential, which is expected because the oxidized form of the 3C-Fc molecule is more conductive than the reduced form. However, the details of the conductance curves are different, displaying three types of behavior: discrete switching from low- to high-conductance levels (type 1, Fig. 3A), an intermediate behavior of continuous increase mixed with large fluctuations (type 2, Fig. 3B), and continuous increase of the conductance with increasing potential (type 3, Fig. 3C). These three types of transient conductance change with potential are also observed for 5C-Fc, 8C-Fc, and 10C-Fc (*SI Appendix*, Fig. S7).

We analyzed the ensemble behavior of the reaction events by constructing 2D histograms of normalized conductance–potential curves for nC-Fc and observed the following trends (Fig. 4A). For each linker length of nC-Fc, the conductance–potential curves are mainly grouped in two bands, a low-conductance band below the equilibrium potential and a high-conductance band above the equilibrium potential, corresponding to the reduced and oxidized states, respectively. The probability of the molecule switching from the low- to the high-conductance bands increases with increasing overpotential. The overall 2D conductance–potential histograms follow the sigmoidal shape as in the average conductance analysis discussed earlier (Fig. 2), but details of the low (reduced)- and high-conductance (oxidized) bands (Fig. 4A, white ovals) for nC-Fc show a systematic change with the length of the molecular linker. The two bands are short along the potential axis for 3C-Fc, with little overlap in potential, reflecting that most conductance curves belong to type 3 (continuous change) and only a few curves display type 1 behavior (two-level switching events). Increasing the molecular length, the two bands become longer and show increasing overlap in potential, indicative of substantially larger numbers of two-level switching events (type 1), as the length of the molecular linker increases.

As noted, sigmoidal dependence of molecular conductance on potential was reported for a viologen derivative in aqueous solution and interpreted using a soft gate model (15). The observation of discrete switching between the reduced and oxidized states, however, makes soft gating a less likely mechanism in the present case. In general, the charge transfer mechanism in molecules depends on microscopic details and solvent (42, 43), as the latter affects the (re)polarization energy and viscosity (44),
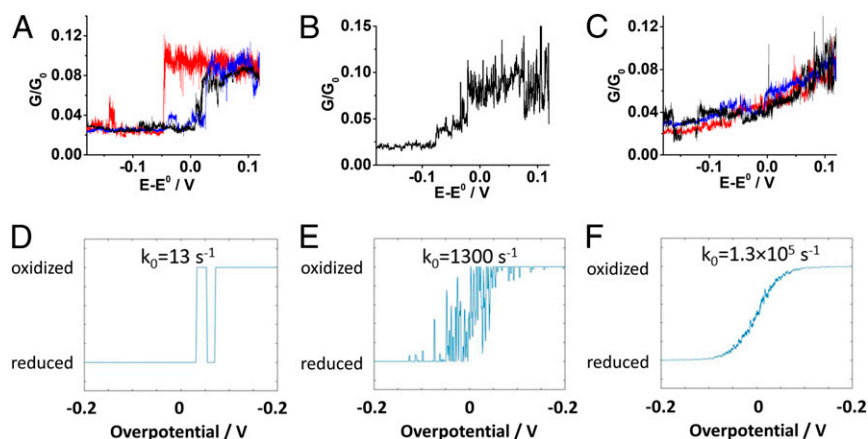
**Fig. 3.** Measured and simulated conductance vs. potential sweeps for single molecules. (*A–C*) Conductance vs. potential of single 3C-Fc molecules: (*A*) discrete two-level, (*B*) intermediate, and (*C*) continuous variations of conductance with potential. The red, blue, and black colors in *A* and *C* represent different sweeps of potential. For clarity, only one curve is shown in *B*. (*D–F*) Simulations of conductance vs. potentials with standard rate constant of (*D*) 13 s$^{-1}$, (*E*) 1,300 s$^{-1}$, and (*F*) 1.3 × 10$^5$ s$^{-1}$. The curves are filtered with a low-pass filter with a cutoff frequency of 500 Hz. Potential sweep rate: 1 V/s.

which are in turn reflected in well-known ways in the interfacial electrochemical electron transfer rate constants (1).

To rationalize the observed three types of conductance change patterns and the systematic length dependence of the 2D conductance–potential histogram, we express the transient conductance of a nC-Fc molecule as

$$G(t, V) = G_{ox}a_{ox}(t, E - E_0) + G_{red}a_{red}(t, E - E_0),\qquad[5]$$

where $a_{ox}$ and $a_{red}$ describe the state of the molecule in the oxidized and reduced states, respectively. $a_{ox}$ and $a_{red}$ change stochastically with time, but obey the rule that $a_{ox} = 1$ if $a_{red} = 0$, and $a_{ox} = 0$ if $a_{red} = 1$. Eq. **5** shows that the conductance of the molecule switches between two levels, depending on $a_{ox}$ and $a_{red}$. The probability for a redox switching event (changes of $a_{ox}$ and $a_{red}$) to occur within a time interval ($\Delta t$) is

$$P(t) = k\Delta t,\qquad[6]$$

where $k$ is the oxidation (or reduction) rate constant. $k$ depends on the potential and follows the Butler–Volmer relation (45),

$$k = k_0 \cdot e^{\left(\mp\frac{1}{2}(E - E_0)/k_B T\right)},\qquad[7]$$

where $k_0$ is the standard rate constant. A negative exponent corresponds to oxidation and a positive exponent to reduction. $P(t)$ based on Eqs. **6** and **7** is plotted against overpotential in *SI Appendix*, Fig. S8*A*. A more accurate expression of rate constant is given by the theories of Kuznetsov (1), Chidsey (46), Dogonadze (47), and Levich (48). However, the reorganization free energy for Fn (∼0.85 eV) (46) is large compared with the overpotential (<0.2 V) and bias potential (0.1 V); the quadratic free-energy form is reduced to the Butler–Volmer expression (derivation in *SI Appendix*, section 3). The Butler–Volmer expression is thus appropriate and used because of its simplicity.

With Eq. **5**, together with Eqs. **6** and **7**, we simulated the individual conductance switching events vs. potential with different rate constants, $k_0$ (Fig. 3 *D–F*; see *Materials and Methods* for details). As the experiment was performed with a finite bandwidth (0–500 Hz; see *SI Appendix*, Fig. S9 for frequency response tests) for the current amplifier, we applied this low-pass filter to the simulated data. At low potentials, the molecule is in the reduced state and the conductance stays at the low-conductance level. When the potential increases toward the equilibrium potential, the probability of oxidation increases, which is reflected

by the increasing number of switching events. When the potential increases well above the equilibrium potential, the molecule is in the oxidized state and the conductance stays at the high conductance level. For a fixed $k_0$, different runs of simulation display a similar pattern (*SI Appendix*, Fig. S8 *B–D*). However, different $k_0$ leads to different patterns in the conductance–potential curve for a molecule. For small $k_0$, the switching frequency is low compared with the experimental bandwidth and the two-level switching is the dominant feature (Fig. 3*D* and *SI Appendix*, Fig. S10). For large $k_0$, the switching frequency is high compared with the experimental bandwidth and these fast switching events are smeared out, leading to continuous increases of the conductance with overpotential (Fig. 3*F* and *SI Appendix*, Fig. S10). For intermediate $k_0$, high-frequency switching events are smeared out to a continuous background, while low-frequency switching events remain (Fig. 3*E* and *SI Appendix*, Fig. S10).

The simulation results offer an explanation for the different types of conductance switching patterns in Fig. 3 *A–C*. There is a large variability in the conductance of single molecules in the STM break junction experiment, due to a microscopic difference in molecule–electrode contact geometry and possibly in the molecular conformations (49, 50). The variability would lead to a broad distribution in the rate constant, $k_0$. Electron transfer reaction events with large $k_0$ are observed with a continuous increase in the conductance with potential, and those with small $k_0$ are observed with two-level conductance fluctuations.

By comparing the individual potential sweeps with the ensemble average (38), the simulation also explains the systematic change in the 2D histogram of the potential-dependent conductance with the molecular linker length. In Fig. 4*B* we randomly generated conductance–potential curves for each rate constant ($k_0$) and constructed 2D histograms from the individual conductance–potential curves like those shown in Fig. 4*A*. For large $k_0$, the 2D histogram is dominated by a continuous increase of the conductance with increasing potential, following the sigmoidal shape. This resembles the 2D histogram of 3C-Fn (Fig. 4*A*). Decreasing $k_0$ leads to a systematic change in the 2D histogram to a two-level switching behavior (Fig. 4*B*). For small $k_0$, the two-level switching is more apparent, showing conductance bands at two levels, corresponding to the reduced and oxidized states. This resembles 10C-Fn in Fig. 4*A*.

The rate constant ($k_0$) is seen to follow an exponential dependence on the molecular bridge length on one side with a decay constant of 0.66 per CH$_2$ group (*SI Appendix*, Fig. S11). Previous electrochemical studies have reported exponential decay
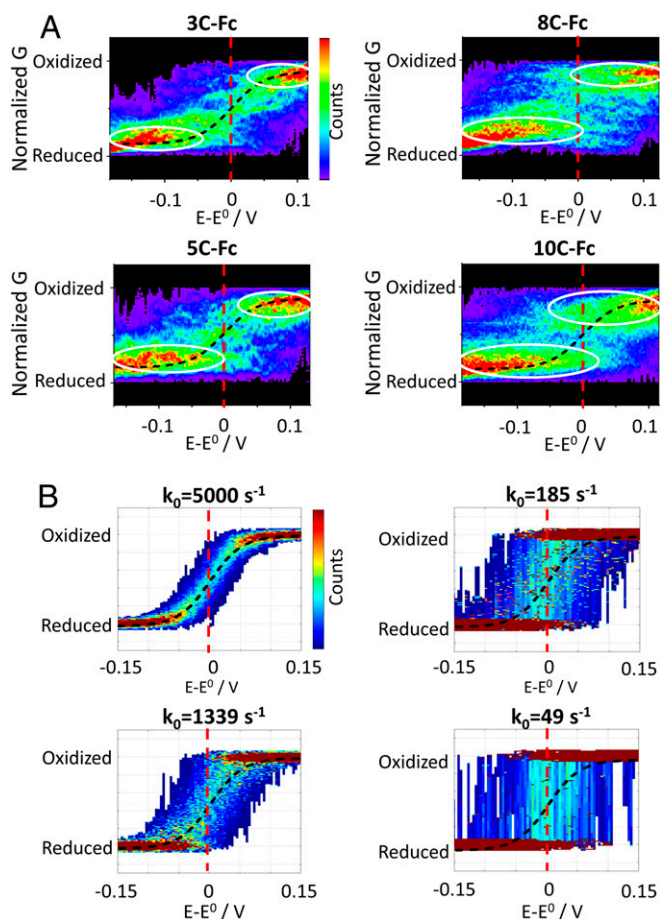
Fig. 4. Statistical analysis of the measured and simulated conductance vs. overpotential sweeps in nC-Fc single molecules. (A) Two-dimensional conductance–potential histograms constructed from over 150 individually measured conductance–potential curves, where the conductances of the reduced and oxidized states are normalized. The vertical dashed lines mark the equilibrium potentials of the ferrocene compounds. The white ovals mark the reduced and oxidized conductance bands. (B) Two-dimensional conductance–potential histograms of 50 individually simulated conductance–potential curves for different standard rate constants (different lengths of the molecular linkers). The sigmoidal dashed lines in A and B are guides for the eye.

of the standard rate constant with the alkane chain length in ferrocene–alkanethiolate self-assembled monolayers (17, 18, 51, 52). To further examine the above model, we studied the length dependence of the average conductance of single nC-Fc molecules in both the oxidized and the reduced states (*SI Appendix*, Fig. S12). Semilogarithmic plots of the conductance in both states decrease linearly with the alkane linker length (number of $CH_2$ groups), showing that the conductance decays exponentially with the molecular length (*SI Appendix*, Fig. S13). The decay constants, $\beta_N$, determined from the slopes of the semilogarithmic plots are $0.69 \pm 0.02$ and $0.65 \pm 0.07$ per $CH_2$ group for the reduced state and the oxidized state, respectively. These decay constants are smaller than those of alkanedithiols without the ferrocene redox center [$\beta_N \sim 1.07 \pm 0.05$ per $CH_2$ group (53); black triangles in *SI Appendix*, Fig. S13]. This observation is consistent with previous reports (21, 54–57) and implies that the inclusion of the redox moiety changes significantly the energy-level alignment of the alkane linkers with respect to the electrode Fermi energy level. This lowers in turn the tunneling barrier height of the alkane linkers and thus leads to a reduced decay constant. Alternatively, the redox center can be viewed as a local indentation (a "hole") in the background tunneling barrier of the alkane linker units.

The exponential conductance dependence on the bridge length is overall consistent with the view that the electron tunnels coherently through nC-Fc, where the redox state switches between reduced and oxidized states. The bias voltage between the STM tip and substrate could potentially affect $\beta_N$, but the bias dependence of the conductance was not studied here due to instability of the single-molecule junctions at high bias voltages.

## Conclusions

We have mapped the transition between single-molecule and averaged macroscopic electronic conductance patterns of a group of nC-Fc molecules covalently enclosed between a gold electrode surface and a gold tip in an electrochemically controlled scanning tunneling microscopy gap. We investigated the interfacial electron transfer reactions in nC-Fc both by measuring the conductance of single molecules and by tracking the individual electron transfer reaction events in one molecule at a time. The average conductance vs. potential follows a sigmoidal dependence, which is quantitatively and most simply described in terms of equilibrium electron transfer and the Nernst equation. This ensemble study shows that measuring of the conductance allows tracking of the redox state of the molecules. The conductance of single molecules exhibits large fluctuations, which reflect the stochastic characteristics of electron transfer reactions. The conductance fluctuations follow a stochastic kinetics model, as shown by numerical simulations and by systematically changing the length of the molecular linker. Ensemble averaging of the individual single-molecule measurements recovers, notably the average conductance behavior. This work shows that individual electron transfer reactions in single molecules can be addressed by monitoring the conductance of the molecules and discloses a transition from the stochastic kinetics of individual reaction events to deterministic thermodynamics of ensemble averages. Observations and results such as these are expected to be of importance in the understanding of chemical reactions in single molecules and small molecular ensembles. This is at the heart of nanoscience, the overarching objective of which is exactly the transition between the single molecule and macroscopic assemblies.

## Materials and Methods

**Immobilization of nC-Fc on Gold Surfaces.** Gold substrates were prepared using an in-house–made ultrahigh-vacuum thin-film deposition system. Before each experiment, the gold substrate was briefly annealed in a hydrogen flame, immediately immersed in mesitylene (98%; Sigma-Aldrich) containing 5 μM nC-Fc, and then incubated overnight. The substrate was then immersed from the mesitylene solution, thoroughly rinsed with mesitylene, and dried with nitrogen gas. The nC-Fc–covered gold substrate was then covered by 0.1 M TBA $BF_4$ (99%; Aldrich) in acetonitrile (99.8%; Alfa Aesar) for electrochemical and conductance measurements.

**Conductance Measurements.** The electrochemical STM break junction experiments were carried out using a Nanoscope E (Digital Instruments Inc.) controller and a Pico-STM scanner (Molecular Imaging). The potentials of the STM tip and substrate electrodes with respect to the reference electrode and the bias voltage between the two electrodes were controlled by a bipotentiostat (Agilent). The STM tip was prepared by cutting a gold wire (0.25 mm diameter, 99.5%; Alfa Aesar) and was coated with Apiezon wax to reduce the leakage current. Apiezon wax is stable and does not dissolve in acetonitrile. A silver wire was used as a quasi-reference electrode and a platinum coil as a counter electrode. Cyclic voltammetry was performed before and after each experiment to determine potential errors due to drift of the quasi-reference electrode over time (*SI Appendix*, Fig. S5).

We performed the electrochemical STM break junction measurements using the following two approaches (20). In the first approach, the STM tip and substrate potentials were fixed with a small bias voltage (100 mV) maintained between the tip and substrate. The STM tip was brought into contact with the substrate and then retracted at a constant speed, during which the conductance vs. distance traces (*SI Appendix*, Fig. S6) were recorded. A plateau in the conductance traces indicated the formation of

single molecules bridged between the STM tip and substrate. After collection of thousands of conductance traces, a conductance histogram (Fig. 2 *A* and *B*) was constructed. The same measurement was then performed at different potentials. In the second approach, the STM tip was brought into contact with the substrate and then retracted from the substrate. When the conductance dropped to a plateau, signaling successful bridging of a molecule between the tip and substrate, the tip position was held fixed and the potential swept at 1 V/s from a negative value to positive values to trigger oxidization of the molecule, during which the conductance vs. potential trace was recorded (Fig. 3 *A*–*C*).

**Simulation Methods.** Individual electron transfer reactions were simulated using MATLAB 2017 based on the following assumptions. The probability for a molecule to be oxidized or reduced over a time interval, $\Delta t$, is given by Eq. **6**. For a small overpotential (much less than reorganization energy), the potential dependence of the reduction and oxidation rate constants is given

by the Butler–Volmer relation (Eq. **7**) (30). We simulated the electron transfer reactions by sweeping the overpotential from −0.2 V to 0.2 V, within which the potential was divided into $0.4 \times 10^6$ bins. The potential sweep rate was chosen according to the experimental sweep rate, 1 V/s, and the time interval for each bin ($\Delta t$) is $10^{-6}$ s. For each bin (potential), we simulated an electron transfer reaction event with a probability determined by Eq. **6**. We repeated the above process for the next bin until reaching 0.2 V for a complete potential sweep. The curve was then filtered with a low-pass filter with a cutoff frequency of 500 Hz. The above simulation was repeated for different $k_0$. We varied the time interval for each bin, $\Delta t$, and performed the same simulation. The pattern of electron transfer reaction during a potential sweep was found to be independent of $\Delta t$ (*SI Appendix*, Fig. S12).

1. Kuznetsov AM, Ulstrup J (1999) *Electron Transfer in Chemistry and Biology. An Introduction to the Theory* (Wiley, Chichester, UK).
2. Dadashi-Silab S, Doran S, Yagci Y (2016) Photoinduced electron transfer reactions for macromolecular syntheses. *Chem Rev* 116:10212–10275.
3. Bard AJ, Faulkner LR (2001) *Electrochemical Methods: Fundamentals and Applications* (Wiley, New York), 2nd Ed.
4. Wang Q, Moerner WE (2014) Single-molecule motions enable direct visualization of biomolecular interactions in solution. *Nat Methods* 11:555–558.
5. Peterman EJG, Wuite GJL (2011) *Single Molecule Analysis: Methods and Protocols* (Humana Press, New York).
6. Cordes T, Blum SA (2013) Opportunities and challenges in single-molecule and single-particle fluorescence microscopy for mechanistic studies of chemical reactions. *Nat Chem* 5:993–999.
7. Janssen KPF, et al. (2014) Single molecule methods for the study of catalysis: From enzymes to heterogeneous catalysts. *Chem Soc Rev* 43:990–1006.
8. Rief M, Gautel M, Oesterhelt F, Fernandez JM, Gaub HE (1997) Reversible unfolding of individual titin immunoglobulin domains by AFM. *Science* 276:1109–1112.
9. Meng CA, Fazal FM, Block SM (2017) Real-time observation of polymerase-promoter contact remodeling during transcription initiation. *Nat Commun* 8:1178.
10. Goldman DH, et al. (2015) Ribosome. Mechanical force releases nascent chain-mediated ribosome arrest in vitro and in vivo. *Science* 348:457–460.
11. Fan F-RF, Bard AJ (1995) Electrochemical detection of single molecules. *Science* 267:871–874.
12. Tao NJ (1996) Probing potential-tuned resonant tunneling through redox molecules with scanning tunneling microscopy. *Phys Rev Lett* 76:4066–4069.
13. Wei C, Bard AJ, Mirkin MV (1995) Scanning electrochemical microscopy. 31. Application of SECM to the study of charge transfer processes at the liquid/liquid interface. *J Phys Chem* 99:16033–16042.
14. Singh PS, Lemay SG (2016) Stochastic processes in electrochemistry. *Anal Chem* 88:5017–5027.
15. Haiss W, et al. (2007) Single-molecule conductance of redox molecules in electrochemical scanning tunneling microscopy. *J Phys Chem B* 111:6703–6712.
16. Xiao X, et al. (2006) Redox-gated electron transport in electrically wired ferrocene molecules. *Chem Phys* 326:138–143.
17. Cheng J, et al. (2001) Distance dependence of the electron-transfer rate across covalently bonded monolayers on silicon. *J Phys Chem B* 105:10900–10904.
18. Smalley JF, et al. (1995) The kinetics of electron transfer through ferrocene-terminated alkanethiol monolayers on gold. *J Phys Chem* 99:13141–13149.
19. Artés JM, López-Martínez M, Díez-Pérez I, Sanz F, Gorostiza P (2014) Conductance switching in single wired redox proteins. *Small* 10:2537–2541.
20. Darwish N, et al. (2012) Single molecular switches: Electrochemical gating of a single anthraquinone-based norbornylogous bridge molecule. *J Phys Chem C* 116:21093–21097.
21. Zhihai L, et al. (2007) Conductance of redox-active single molecular junctions: An electrochemical approach. *Nanotechnology* 18:044018.
22. Ricci AM, Calvo EJ, Martin S, Nichols RJ (2010) Electrochemical scanning tunneling spectroscopy of redox-active molecules bound by Au-C bonds. *J Am Chem Soc* 132:2494–2495.
23. Xiang L, et al. (2017) Gate-controlled conductance switching in DNA. *Nat Commun* 8:14471.
24. Li Y, et al. (2017) Mechanical stretching-induced electron-transfer reactions and conductance switching in single molecules. *J Am Chem Soc* 139:14699–14706.
25. Chi Q, Farver O, Ulstrup J (2005) Long-range protein electron transfer observed at the single-molecule level: In situ mapping of redox-gated tunneling resonance. *Proc Natl Acad Sci USA* 102:16203–16208.
26. Yin X, et al. (2017) A reversible single-molecule switch based on activated antiaromaticity. *Sci Adv* 3:eaao2615.
27. Reimers JR, Ford MJ, Halder A, Ulstrup J, Hush NS (2016) Gold surfaces and nanoparticles are protected by Au(0)-thiyl species and are destroyed when Au(I)-thiolates form. *Proc Natl Acad Sci USA* 113:E1424–E1433.
28. Xu B, Tao NJ (2003) Measurement of single-molecule resistance by repeated formation of molecular junctions. *Science* 301:1221–1223.
29. Liu A, Leese DN, Swarts JC, Sykes AG (2002) Reduction of Escherichia coli ribonucleotide reductase subunit R2 with eight water-soluble ferrocene derivatives. *Inorg Chim Acta* 337:83–90.
30. Kuznetsov AM, Ulstrup J (2000) Mechanisms of in situ scanning tunnelling microscopy of organized redox molecular assemblies. *J Phys Chem A* 104:11531–11540.
31. Albrecht T, Guckian A, Ulstrup J, Vos H (2004) Transistor effects and in situ STM of redox molecules at room temperature. *IEEE Trans Nanotechnol* 4:134–136.
32. Rudnev AV, Pobelov IV, Wandlowski T (2011) Structural aspects of redox-mediated electron tunneling. *J Electroanal Chem* 660:302–308.
33. Schmickler W, Widrig C (1992) The investigation of redox reactions with a scanning tunneling microscope: Experimental and theoretical aspects. *J Electroanal Chem* 336:213–221.
34. Schmickler W, Tao N (1997) Measuring the inverted region of an electron transfer reaction with a scanning tunneling microscope. *Electrochim Acta* 42:2809–2815.
35. Friis EP, Kharkats YI, Kuznetsov AM, Ulstrup J (1998) In situ scanning tunneling microscopy of a redox molecule as a vibrationally coherent electronic three-level process. *J Phys Chem A* 102:7851–7859.
36. Galperin M, Ratner MA, Nitzan A (2005) Hysteresis, switching, and negative differential resistance in molecular junctions: A polaron model. *Nano Lett* 5:125–130.
37. Kuznetsov AM, Ulstrup J (1994) Scanning tunnelling microscopy currents through large adsorbate molecules as a molecular three-centre electronic process. *Surf Coat Tech* 67:193–200.
38. Migliore A, Nitzan A (2013) Irreversibility and hysteresis in redox molecular conduction junctions. *J Am Chem Soc* 135:9420–9432.
39. Schwarz F, et al. (2016) Field-induced conductance switching by charge-state alternation in organometallic single-molecule junctions. *Nat Nanotechnol* 11:170–176.
40. Yuan L, et al. (2018) Transition from direct to inverted charge transport Marcus regions in molecular junctions via molecular orbital gating. *Nat Nanotechnol* 13:322–329.
41. Kuznetsov AM (2007) Negative differential resistance and switching behavior of redox-mediated tunnel contact. *J Chem Phys* 127:084710.
42. Osorio HM, et al. (2015) Electrochemical single-molecule transistors with optimized gate coupling. *J Am Chem Soc* 137:14319–14328.
43. Nichols RJ, Higgins SJ (2016) Single molecule nanoelectrochemistry in electrical junctions. *Acc Chem Res* 49:2640–2648.
44. Yu G, Zhao D, Wen L, Yang S, Chen X (2011) Viscosity of ionic liquids: Database, observation, and quantitative structure-property relationship analysis. *AIChE J* 58:2885–2899.
45. Bockris JOM, Reddy AKN, Gamboa-Aldeco ME (2000) *Modern Electrochemistry 2A-Fundamentals of Electrodics* (Springer, New York).
46. Chidsey CED (1991) Free energy and temperature dependence of electron transfer at the metal-electrolyte interface. *Science* 251:919–922.
47. Dogonadze RR (1971) Reactions of molecules at electrodes. *Theory of Molecular Electrode Kinetics*, ed Hush NS (Wiley, New York), pp 135–227.
48. Levich VG (1966) *Advances in Electrochemistry and Electrochemical Engineering*, ed Delahay P (Wiley Interscience, New York), pp 249–371.
49. Lawson JW, Bauschlicher CW (2006) Transport in molecular junctions with different metallic contacts. *Phys Rev B* 74:125401.
50. Guo S, Hihath J, Díez-Pérez I, Tao N (2011) Measurement and statistical analysis of single-molecule current-voltage characteristics, transition voltage spectroscopy, and tunneling barrier height. *J Am Chem Soc* 133:19189–19197.
51. Weber K, Hockett L, Creager S (1997) Long-range electronic coupling between ferrocene and gold in alkanethiolate-based monolayers on electrodes. *J Phys Chem B* 101:8286–8291.
52. Sumner JJ, Weber KS, Hockett LA, Creager SE (2000) Long-range heterogeneous electron transfer between ferrocene and gold mediated by n-alkane and N-alkyl-carboxamide bridges. *J Phys Chem B* 104:7449–7454.
53. Li X, et al. (2006) Conductance of single alkanedithiols: Conduction mechanism and effect of molecule-electrode contacts. *J Am Chem Soc* 128:2135–2141.
54. Lu Q, Yao C, Wang X, Wang F (2012) Enhancing molecular conductance of oligo(p-phenylene ethynylene)s by incorporating ferrocene into their backbones. *J Phys Chem C* 116:17853–17861.
55. Getty SA, et al. (2005) Near-perfect conduction through a ferrocene-based molecular wire. *Phys Rev B* 71:241401.
56. Sun Y-Y, et al. (2014) Enhancing electron transport in molecular wires by insertion of a ferrocene center. *Phys Chem Chem Phys* 16:2260–2267.
57. Winkler JR, Gray HB (2014) Long-range electron tunneling. *J Am Chem Soc* 136:2930–2939.